



Cite this: *Chem. Sci.*, 2021, 12, 2404

All publication charges for this article have been paid for by the Royal Society of Chemistry

# Tandem diaza-Cope rearrangement polymerization: turning intramolecular reaction into powerful polymerization to give enantiopure materials for Zn<sup>2+</sup> sensors†

Soon-Hyeok Hwang and Tae-Lim Choi \*

[3,3]-Sigmatropic rearrangement is a powerful reaction to form C–C bonds stereospecifically; however, owing to intrinsic simultaneous bond formation and breakage, this versatile method has not been utilized in polymerization. Herein, we report a new tandem diaza-Cope rearrangement polymerization (DCRP) that can synthesize polymers with defect-free C–C bond formation from easy and efficient imine formation. A mechanistic investigation by *in situ* <sup>1</sup>H NMR experiments suggests that this polymerization proceeds by a rapid DCR process, forming an enantiospecific C–C bond that occurs almost simultaneously with imine formation. This polymerization produces not only highly stable polymers against hydrolysis due to resonance-assisted hydrogen bonds (RAHBs) but also chiral polymers containing enantiopure salen moieties, which lead to high-performance Zn<sup>2+</sup>-selective turn-on chemosensors with up to 73-fold amplification. We also found that their optical activities and sensing performances are heavily dependent on the reaction temperature, which significantly affects the stereoselectivity of DCR.

Received 8th November 2020  
Accepted 1st December 2020

DOI: 10.1039/d0sc06138g

rsc.li/chemical-science

## Introduction

Pericyclic reaction, the reorganization of  $\pi$ -bonds in a concerted manner, is one of the most widely used transformations in synthetic organic chemistry. Among the various pericyclic reactions, highly efficient cycloadditions, such as Diels–Alder and Cu-catalyzed azide–alkyne cycloaddition reactions, have been employed as powerful tools to prepare polymers<sup>1–10</sup> because of their high efficiency and orthogonality (Scheme 1A(a)). [3,3]-Sigmatropic rearrangement is another powerful and reliable pericyclic reaction, allowing for the stereoselective construction of C–C bonds.<sup>11</sup> However, this rearrangement cannot be applied to polymerization other than the post-modification of side-chains<sup>12–16</sup> because it is an intramolecular reaction, which intrinsically forms and breaks the bond simultaneously (Scheme 1A(b)).

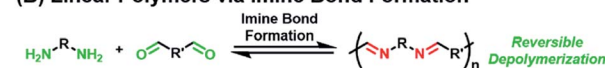
Meanwhile, imine formation between an amine and an aldehyde is an efficient and straightforward reaction and occurs reversibly under equilibrium control. Taking advantage of this dynamic nature, imine formation is widely employed for synthesizing polyimine vitrimers,<sup>17–22</sup> rotaxanes, and catenanes.<sup>23,24</sup> Ironically, extending this method to obtain high-

molecular-weight linear polymers is still quite challenging due to its inherent reversible imine formation (Scheme 1B).<sup>25–38</sup> Therefore, to solve the depolymerization issue, an

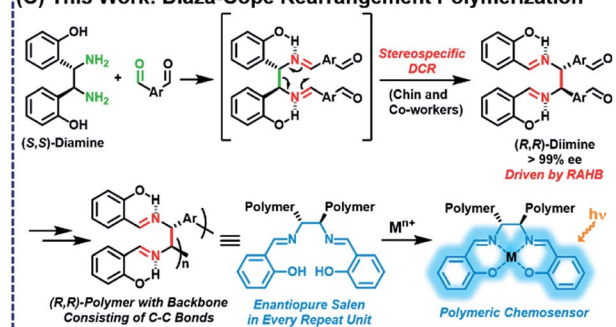
### (A) Pericyclic Reactions



### (B) Linear Polymers via Imine Bond Formation



### (C) This Work: Diaza-Cope Rearrangement Polymerization



Scheme 1 Polymerization via pericyclic reactions and imine formation.

Department of Chemistry, Seoul National University, Seoul 08826, Korea. E-mail: tlc@snu.ac.kr

† Electronic supplementary information (ESI) available. See DOI: 10.1039/d0sc06138g





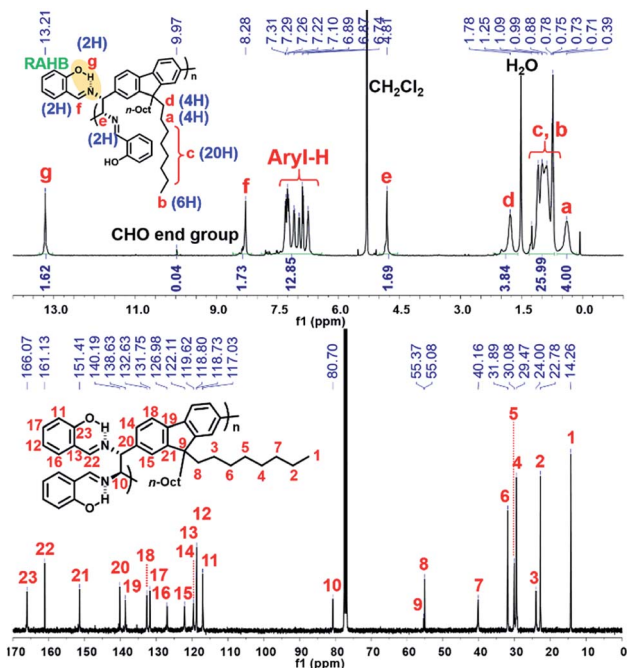


Fig. 1  $^1\text{H}$  NMR and  $^{13}\text{C}$  NMR spectra of  $(R,R)$ -P1.

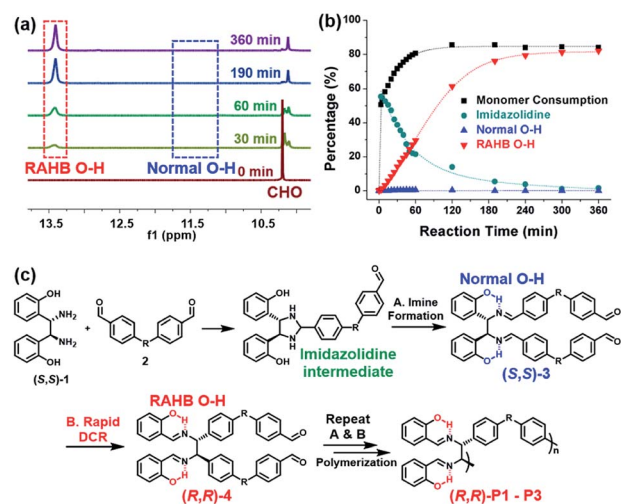


Fig. 2 (a) Monitoring the polymerization using  $(S,S)$ -1 and **2a** by *in situ*  $^1\text{H}$  NMR spectroscopy in  $\text{DMF-}d_7$ . (b) Plots showing consumption of **2a** (black), formation of the imidazolidine intermediate (green), and phenolic O–H groups (blue and red). (c) Detailed polymerization mechanism.

intermediate *via* imine formation was rapidly formed up to 55% (see Fig. S1† for details).<sup>46,47</sup> However,  $(S,S)$ -3, the second intermediate, comprising the normal O–H signal, was hardly observed, whereas only the RAHB O–H signal corresponding to  $(R,R)$ -4 or  $(R,R)$ -P1 gradually increased, implying clean conversion (Fig. 2a and b). This suggests that a DCR is rapid, occurring almost simultaneously with imine formation (Fig. 2c). In other words,  $(R,R)$ -P1 was predominantly produced by C–C bond polymerization rather than imine polymerization (if so, the

subsequent DCR process would have slowly generated C–C bonds on the pre-formed polymer). On the other hand, in the case of  $(R,R)$ -P2 containing electron-donating groups, the activation energy for DCR increased,<sup>42</sup> thereby decelerating the rearrangement. As a result, both normal and RAHB O–H ( $\delta$  10.7 ppm and  $\delta$  13.7 ppm, respectively) were observed at the beginning of the reaction, but the polymerization progressed to show only the enthalpically favored RAHB O–H (Fig. S2†). In short, because of the defect-free DCR signal regardless of the electronic characters, this tandem DCRP becomes a novel strategy to form more challenging C–C bonds from easier imine formation.

DCR polymers contain C–C bonds in the main backbone, while the resulting imine bonds at the side-chains are also stabilized by stronger RAHBs. Therefore, we could test their stability against hydrolysis by comparing with analogous poly-imine. To conduct a control experiment, we synthesized **P4** by using a diamine monomer ( $(S,S)$ -7) without –OH groups, ensuring that the RAHB that drove the completion of DCR was now absent.<sup>39</sup> Therefore, **P4** ( $M_n$  of 14.1 kDa) contained both the initial imine ( $(S,S)$ -8) and the rearranged C–C bond ( $(R,R)$ -9) in the main chain (Fig. 3a). As expected, **P4** in the THF solution containing 1%  $\text{H}_2\text{O}$  underwent depolymerization, lowering  $M_n$  to 5.4 kDa within a day. After three days, **P4** was further hydrolyzed to 3.6 kDa, which is 1/4 of the initial molecular weight (Fig. 3b). However, as shown by SEC analysis, the molecular weight of  $(R,R)$ -P1 from the complete DCRP did not change under identical conditions even after seven days (Fig. 3c). Moreover,  $(R,R)$ -P1 remained stable in  $\text{CDCl}_3$  in an NMR tube for three days, but even a small amount of residual acid in  $\text{CDCl}_3$  was sufficient to depolymerize **P4** within 11 h, as seen by the reduction in the imine signal ( $\delta$  8.3 ppm) and the significant increase in the aldehyde signal ( $\delta$  10.0 ppm) (Fig. S3†).

The DCR of small molecules undergoes complete stereo-specific inversion of stereochemistry at rt because the corresponding transition state (TS) bears all the aryl substituents in pseudo-equatorial positions making this pathway most

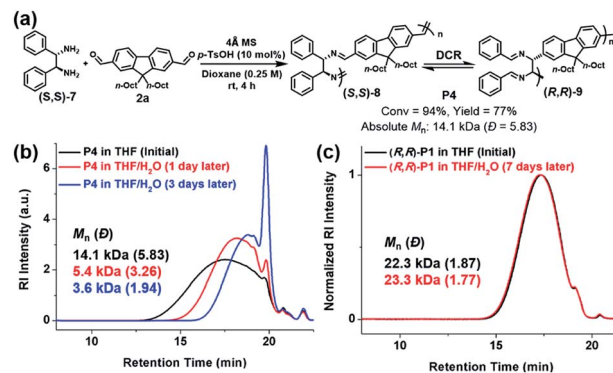


Fig. 3 Control experiment to compare stability against hydrolysis. (a) Scheme for **P4**. (b) SEC traces of **P4** measured at the initial and measured one/three days after dissolving in THF :  $\text{H}_2\text{O}$  (99 : 1). (c) SEC traces of  $(R,R)$ -P1 measured at the initial and seven days after dissolving in THF :  $\text{H}_2\text{O}$  (99 : 1).

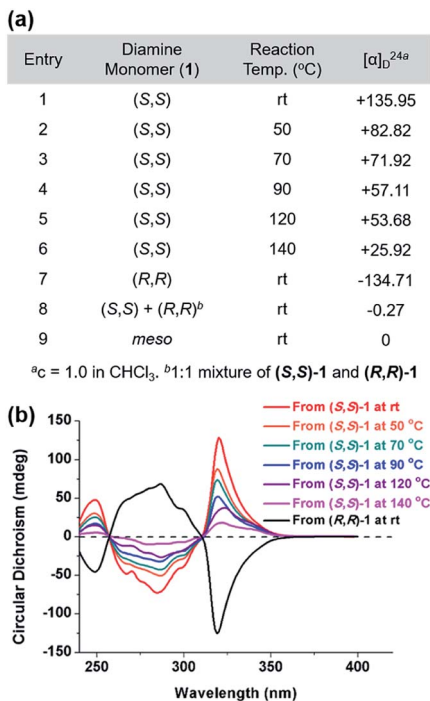


Fig. 4 (a) Table for optical rotation values showing how temperature affects the stereospecificity of tandem DCRP. (b) Circular dichroism spectra of the resulting polymers (2.5 mg mL<sup>-1</sup> in CHCl<sub>3</sub> at rt, 0.2 mm cell).

kinetically preferred.<sup>42</sup> Likewise, to investigate the stereochemistry of the resulting polymers, we prepared **P1** at various temperatures and compared their optical rotations ( $[\alpha]_D^{24}$ ) (Fig. 4a and Table S4<sup>†</sup>). While **P1** synthesized from (S,S)-1 at rt exhibited the highest  $[\alpha]_D^{24}$  of +135.95, the values significantly decreased from +82.82 to +25.92 as the polymerization temperature increased from 50 °C to 140 °C (entries 1–6 in Fig. 4a). In addition, (S,S)-**P1** obtained from the enantiomer (R,R)-1 at rt (entry 8 in Table 1) showed an expected  $[\alpha]_D^{24}$  of similar absolute value but the opposite sign (–134.71) (entry 7 in Fig. 4a). Lastly, **P1** prepared from the racemic mixture or *meso*-isomer of **1** resulted in  $[\alpha]_D^{24}$  close to 0 (entries 8 and 9 in Fig. 4a). To further support this trend, we measured circular dichroism spectra, which showed a decrease in the amplitudes of the two Cotton effects with an increase in the reaction temperature (Fig. 4b). Furthermore, (R,R)-**P1** and (S,S)-**P1** synthesized at rt showed Cotton effects of the same amplitude but of the opposite sign. According to the computational studies, the next alternating pathway *via* the second lowest TS (7.7 kcal mol<sup>-1</sup> higher) would produce a *meso* product, an achiral diastereomer.<sup>42</sup> Therefore, it is suspected that the higher reaction temperature led to more *meso* products in **P1**, thereby lowering  $[\alpha]_D^{24}$  and the amplitude of Cotton effects accordingly.

To confirm the effect of temperature on *meso*-isomer formation, we thoroughly analyzed the <sup>1</sup>H-NMR spectra of **P1** from (S,S)-1 and *meso*-**P1** synthesized at various temperatures (Fig. 5a and S4<sup>†</sup>). As the polymerization temperature increased, another peak labeled as *g'* appeared and gradually increased at  $\delta$  13.38 ppm (Fig. 5a and S4a–f<sup>†</sup>). Notably, apart from the *g* and

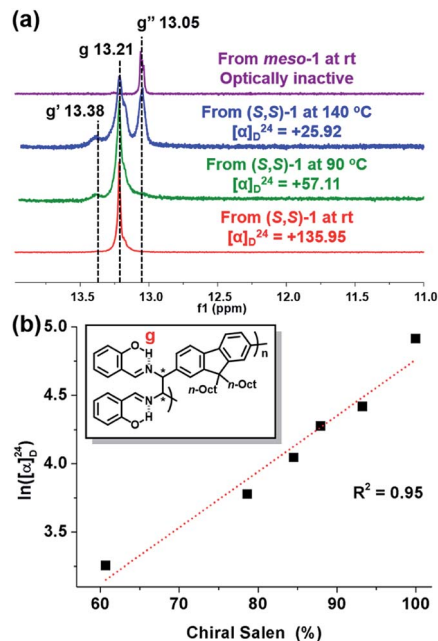


Fig. 5 (a) <sup>1</sup>H NMR spectra (in CD<sub>2</sub>Cl<sub>2</sub>) showing RAHB O–H signals of various **P1** (in Table S4<sup>†</sup>) synthesized from chiral and *meso* diamines at various reaction temperatures. (b) Plot showing the relationship between  $\ln([\alpha]_D^{24})$  and stereospecificity.

*g'* peaks, an additional RAHB O–H signal (*g''* at  $\delta$  13.05 ppm) started to grow for **P1** synthesized at higher temperatures. Fortunately, the last *g''* peak was easily identified as the *meso* diastereomer as it perfectly matched with the authentic sample of *meso*-**P1** prepared from *meso*-1 at rt (Fig. 5a and S4g<sup>†</sup>). From these data, we came to a plausible conclusion that the three types of RAHB O–H signals are due to diad tacticities of the salen side-chains in the following cases: (i) *g* for the homo diad (cm<sup>3</sup>) from the chiral-salen-rich units; (ii) *g''* for the homo diad (mm) from the achiral *meso*-salen-rich units; (iii) *g'* for the hetero diad (cm) from the chiral and *meso*-salen-rich units adjacent to each other. Based on this assignment, the content of the chiral salen unit depending on the temperature was estimated from the integration of all RAHB O–H signals (Fig. S5a<sup>†</sup>). Consistent with the trend observed in  $[\alpha]_D^{24}$ , the chiral salen content also decreased from 100% to 60.7% as the temperature increased from rt to 140 °C. Moreover, one could plot  $[\alpha]_D^{24}$  to the chiral content, and they showed an exponential relationship (Fig. S5b<sup>†</sup>). Taking the natural logarithm of  $[\alpha]_D^{24}$  provided a good linear relationship with the chiral content, which should allow for some predictability (Fig. 5b). In short, increasing the reaction temperature lowered the stereospecificity as well as  $[\alpha]_D^{24}$  due to the formation of the *meso*-isomer.

One useful application of salen moieties is their potential as a metal chemosensor.<sup>48–50</sup> Since (R,R)-**P1**–**P3** contain salen side-chains, their UV/vis absorption and fluorescence responses to various metal cations in THF/H<sub>2</sub>O (9 : 1 v/v) were investigated (Fig. 6 and S8–S12<sup>†</sup>). Interestingly, all the metal cations showed insignificant fluorescence except for Zn<sup>2+</sup>, which showed obvious turn-on fluorescence enhancement ( $I - I_0$ ) (Fig. 6a, b and S8<sup>†</sup>). On the other hand, no sensing ability was observed





- 10 P. Fuchs, P. Vana and K. Zhang, *J. Polym. Sci.*, 2020, **58**, 1535–1543.
- 11 E. A. Ilardi, C. E. Stivala and A. Zakarian, *Chem. Soc. Rev.*, 2009, **38**, 3133–3148.
- 12 G. Yang, S.-i. Matsuzono, E. Hoyama, H. Tokuhisa and K. Hiratani, *Macromolecules*, 2001, **34**, 6545–6547.
- 13 W. Wang, X. Qi, Y. Guan, F. Zhang, J. Zhang, C. Yan, Y. Zhu and X. Wan, *J. Polym. Sci., Part A: Polym. Chem.*, 2016, **54**, 2050–2059.
- 14 A. Tena, S. Rangou, S. Shishatskiy, V. Filiz and V. Abetz, *Sci. Adv.*, 2016, **2**, e151859.
- 15 D. Meis, A. Tena, S. Neumann, P. Georgopoulos, T. Emmeler, S. Shishatskiy, S. Rangou, V. Filiz and V. Abetz, *Polym. Chem.*, 2018, **9**, 3987–3999.
- 16 M. R. d. I. Viuda, A. Tena, S. Neumann, S. Willruth, V. Filiz and V. Abetz, *Polym. Chem.*, 2018, **9**, 4007–4016.
- 17 P. Taynton, C. Zhu, S. Loob, R. Shoemaker, J. Pritchard, Y. Jin and W. Zhang, *Polym. Chem.*, 2016, **7**, 7052–7056.
- 18 S. Zhang, Y. Lv, L. Zheng, J. Li, S. Liang, Z. Liu and L. Ren, *J. Bionic Eng.*, 2017, **14**, 119–129.
- 19 H. Zheng, Q. Liu, X. Lei, Y. Chen, B. Zhang and Q. Zhang, *J. Polym. Sci., Part A: Polym. Chem.*, 2018, **56**, 2531–2538.
- 20 R. Mo, J. Hu, H. Huang, X. Sheng and X. Zhang, *J. Mater. Chem. A*, 2019, **7**, 3031–3038.
- 21 S. Wang, S. Ma, Q. Li, X. Xu, B. Wang, K. Huang, Y. Liu and J. Zhu, *Macromolecules*, 2020, **53**, 2919–2931.
- 22 R. Hajji, A. Duval, S. Dhers and L. Avérous, *Macromolecules*, 2020, **53**, 3796–3805.
- 23 C. D. Meyer, C. S. Joiner and J. F. Stoddart, *Chem. Soc. Rev.*, 2007, **36**, 1705–1723.
- 24 M. E. Belowich and J. F. Stoddart, *Chem. Soc. Rev.*, 2012, **41**, 2003–2024.
- 25 C. S. Marvel and N. Tarköy, *J. Am. Chem. Soc.*, 1957, **79**, 6000–6002.
- 26 K. Suematsu, K. Nakamura and J. Takeda, *Polym. J.*, 1983, **15**, 71–79.
- 27 K.-S. Lee and J. C. Won, *Makromol. Chem.*, 1989, **190**, 1547–1552.
- 28 S.-B. Park, H. Kim, W.-C. Zin and J. C. Jung, *Macromolecules*, 1993, **26**, 1627–1632.
- 29 C.-J. Yang and S. A. Jenekhe, *Macromolecules*, 1995, **28**, 1180–1196.
- 30 W. Sun, X. Gao and F. Lu, *Appl. Polym. Sci.*, 1997, **64**, 2309–2315.
- 31 O. Thomas, O. Inganäs and M. R. Andersson, *Macromolecules*, 1998, **31**, 2676–2678.
- 32 S. Destri, M. Pasini, C. Pelizzi, W. Porzio, G. Predieri and C. Vignali, *Macromolecules*, 1999, **32**, 353–360.
- 33 S. C. Suh and S. C. Shim, *Synth. Met.*, 2000, **114**, 91–95.
- 34 O. Catanescu, M. Grigoras, G. Colotin, A. Dobreanu, N. Hurduc and C. I. Simionescu, *Eur. Polym. J.*, 2001, **37**, 2213–2216.
- 35 H.-J. Niu, Y.-D. Huang, X.-D. Bai and X. Li, *Mater. Lett.*, 2004, **58**, 2979–2983.
- 36 M. Grigoras and C. O. Catanescu, *J. Macromol. Sci., Polym. Rev.*, 2004, **44**, 131–173.
- 37 J. C. Hindson, B. Ulgut, R. H. Friend, N. C. Greenham, B. Norder, A. Kotlewski and T. J. Dingemans, *J. Mater. Chem.*, 2010, **20**, 937–944.
- 38 A. Iwan, M. Palewicz, A. Chuchmala, L. Gorecki, A. Sikora, B. Ma-zurek and G. Pasciak, *Synth. Met.*, 2012, **162**, 143–153.
- 39 J. Chin, F. Mancin, N. Thavarajah, D. Lee, A. Lough and D. S. Chung, *J. Am. Chem. Soc.*, 2003, **125**, 15276–15277.
- 40 H.-J. Kim, H. Kim, G. Alhakimi, E. J. Jeong, N. Thavarajah, L. Stud-nicki, A. Koprianiuk, A. J. Lough, J. Suh and J. Chin, *J. Am. Chem. Soc.*, 2005, **127**, 16370–16371.
- 41 H.-J. Kim, W. Kim, A. J. Lough, B. M. Kim and J. Chin, *J. Am. Chem. Soc.*, 2005, **127**, 16776–16777.
- 42 H. Kim, Y. Nguyen, C. P.-H. Yen, L. Chagal, A. J. Lough, B. M. Kim and J. Chin, *J. Am. Chem. Soc.*, 2008, **130**, 12184–12191.
- 43 H. Kim, Y. Nguyen, A. J. Lough and J. Chin, *Angew. Chem., Int. Ed.*, 2008, **47**, 8678–8681.
- 44 D.-N. Lee, H. Kim, L. Mui, S.-W. Myung, J. Chin and H.-J. Kim, *J. Org. Chem.*, 2009, **74**, 3330–3334.
- 45 H. Kim, M. Staikova, A. J. Lough and J. Chin, *Org. Lett.*, 2009, **11**, 157–160.
- 46 S. H. Kwon, S. M. Lee, S. M. Byun, J. Chin and B. M. Kim, *Org. Lett.*, 2012, **14**, 3664–3667.
- 47 M. Kim, H. Kim, H. Kim and J. Chin, *J. Org. Chem.*, 2017, **82**, 12050–12058.
- 48 Y. Xu, J. Meng, L. Meng, Y. Dong, Y. Cheng and C. Zhu, *Chem.–Eur. J.*, 2010, **16**, 12898–12903.
- 49 J. Li, Y. Wu, F. Song, G. Wei, Y. Cheng and C. Zhu, *J. Mater. Chem.*, 2012, **22**, 478–482.
- 50 M. K. Bera, C. Chakraborty and S. Malik, *New J. Chem.*, 2015, **39**, 9207–9214.

